ACS BIO & MED CHEM Au
AN OPEN ACCESS JOURNAL OF THE AMERICAN CHEMICAL SOCIETY

pubs.acs.org/biomedchemau

Article

Exosome-Encased Nucleic Acid Scaffold Chemotherapeutic Agents for Superior Anti-Tumor and Anti-Angiogenesis Activity

Ryan P. McNamara, Anthony B. Eason, Yijun Zhou, Rachele Bigi, Jack D. Griffith, Lindsey M. Costantini, Michelle A. Rudek, Nicole M. Anders, Blossom A. Damania, and Dirk P. Dittmer*

Cite This: *ACS Bio Med Chem Au* 2022, 2, 140–149

Read Online

ACCESS | Metrics & More | Article Recommendations | Supporting Information

ABSTRACT: Extracellular vesicles (EVs), or exosomes, play a pivotal role in tumor growth and metastasis, such as in the case of Kaposi Sarcoma. By loading tumor-derived EVs with chemotherapeutic drugs, we noted that their pro-tumor/pro-angiogenic phenotype was converted into an anti-tumor phenotype *in vivo*. Drug concentration in EVs was significantly higher than in clinically approved liposome formulation, as retention was facilitated by the presence of miRNAs inside the natural EVs. This demonstrates a new mechanism by which to increase the payload capacity of nanoparticles. By exploiting the targeting preferences of tumor-derived EVs, chemotherapeutics can be directed to specifically poison the cells and the microenvironment that enables metastasis.

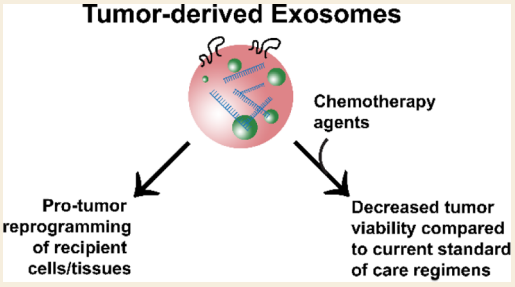

KEYWORDS: *exosome, extracellular vesicles, drug delivery, Kaposi's sarcoma, virology*

INTRODUCTION

Extracellular vesicles (EVs), such as exosomes and microvesicles, have received considerable attention in recent years (reviewed in ref 1). EVs are secreted by all cell types and circulate at high concentrations in body fluids such as blood, lymph, and interstitial and tumor effusions.[2−4] EVs contain specific surface markers, such as the tetraspanin CD81, and selectively incorporate miRNAs from the cell of origin. Therefore, EVs have long been explored as biomarkers of disease.[5−8] More recent studies are starting to explore their use as therapeutics and novel delivery vehicles.

EVs play a pivotal role in remodeling the tumor microenvironment and priming distant tissues for metastasis, as they possess organ-specific homing abilities.[9] This prompted our hypothesis to exploit the naturally evolved tissue-specific homing abilities of tumor-derived EVs to deliver chemotherapeutic drugs to the sites of distant metastases. There are two differences between EVs and artificial liposomes. First, EVs contain proteins and a much more complex composition of lipids. These are believed to aid in tissue-specific targeting and fusion abilities. They may also shield natural EVs from premature clearance in the blood stream. Second, EVs contain micro RNAs (miRNAs) and other nucleic acids. These nucleic acids typically fold into complex structures driven by vertical base-stacking interactions and "horizontal" base-pairing interactions. We hypothesized that the EV-encased miRNAs can act as molecular sponges for nucleic acid-intercalating chemotherapeutic drugs, such as doxorubicin. Once diffused inside the EVs, these compounds would bind the miRNAs, thus driving the equilibrium toward drug-loaded EVs. Even some cancer chemotherapy drugs, such as paclitaxel, that have a mechanism of action that does not involve DNA interaction nevertheless can bind to nucleic acids.[10] As the drug-loaded EVs retain their intrinsic cell lineage-targeting capacity, this allows for a high drug dose to be delivered specifically to just those cells that enable tumor growth and metastasis.

To test this hypothesis, we chose primary effusion lymphoma (PEL), which is caused by Kaposi Sarcoma-associated herpesvirus (KSHV). KSHV also is the causative agent of Kaposi Sarcoma (KS), one of the most angiogenic and disseminated cancers known in humans. Paracrine mechanisms are pivotal to both PEL and KS tumorigenesis and metastasis (reviewed in ref 11). We had shown earlier that PEL secretes high concentrations of EVs, which we term KSHV-EVs. These contain tumor-derived miRNAs at high concentrations. In the case of PEL, the majority of EV-encased miRNAs are of viral origin. KSHV-EVs circulate systemically and are readily detectable in a patient's pleural fluid and plasma, and KSHV-EVs reprogram naïve, uninfected endothelial cells through the delivery of the viral miRNAs which promotes tumor angiogenesis.[6,12,13]

The first line of treatment for KS and PEL is pegylated liposomal doxorubicin (Doxil), and the second line of treatment for KS is paclitaxel (PTX). In low- and middle-income countries, where Doxil is not available or not affordable, free doxorubicin

Received: August 10, 2021
Revised: November 29, 2021
Accepted: November 29, 2021
Published: January 20, 2022

https://doi.org/10.1021/acsbiomedchemau.1c00030
ACS Bio Med Chem Au 2022, 2, 140–149

(DOX) is used for the treatment of KS and PEL. DOX and PTX have differing but well-understood mechanisms of action. Hence, DOX and PTX were used for these studies. Doxil afforded us a clinically relevant control against which to measure the activity of the drug-loaded KSHV-EVs. Indeed, DOX-loaded KSHV-EVs proved superior to Doxil in terms of the drug-load capacity and reducing tumor cell viability. Drug-binding to miRNAs within the tumor-derived EVs was demonstrated as the mechanism of action for these phenotypes.

EXPERIMENTAL SECTION

Cell Lines

U2OS (osteosarcoma) and human embryonic kidney (HEK) 293 cells were grown in Dulbecco's modified Eagle medium supplemented with 10% EV-free fetal bovine serum (FBS), 100 U/mL penicillin, and 100 μg/mL streptomycin. Cells were grown inside tissue-culture flasks in a 37 °C incubator maintained at 5% CO_2. BCBL1 (KSHV-driven B-cell lymphoma) cells were grown in Roswell Park Memorial Institute (RPMI) medium under the same conditions. Human telomerase reverse transcriptase human umbilical vein endothelial cells (hTERT-HUVEC) were grown in EGM-2 media with EV-free FBS under the conditions mentioned above. KSHV-chronically infected hTERT-HUVEC cells were grown in EGM-2 media with EV-free FBS under the conditions mentioned above or as previously described.[13] TALON Dicer KO HEK 293T cells were previously described.[14] All cells were from the American Type Culture Collection (ATCC) or the AIDS Cancer Specimen Resource (ACSR). DICER-KO BCBL-1 cells were generated in this study and were STR-typed using a PROMEGA kit and periodically tested for mycoplasma.

Patient Fluid Processing

PEL fluid and plasma from a healthy donor (HD) were obtained and clarified through initial centrifugation at 1,200×g at 4 °C for 15 min. The fluid was then successively passed through 0.45 μm (Fisher 13-100-107) and 0.22 μm syringe filters (Genesee 25-244). Total EVs were precipitated out of solution with 40 mg/mL polyethylene glycol (PEG-8000) (Fisher 156-500) diluted in 1× phosphate buffered saline (PBS). Clinical material was from public repositories (red cross). Therefore, this research was classified as non-human subject research by the institutional review board of the University of North Carolina at Chapel Hill.

Cell and EV Lysis and Immunoblotting

The whole-cell lysate was divided up into soluble/cytoplasmic and insoluble/chromatin fractions using non-reducing passive lysis buffer (1% NP-40, 5% glycerol), 150 mM NaCl, 20 mM Tris-HCl pH = 7.5, 1 mM phenylmethylsulphonyl fluoride (PMSF), a 1× ETDA-free protease inhibitor (Sigma-Aldrich 11873580001), and 1.5 mM $MgCl_2$. Cells were resuspended in the passive lysis buffer and incubated at 4 °C for 30 min and then spun at 10,000×g for 10 min. The soluble/cytoplasmic fraction was placed into two separate tubes, one containing 1 mM dithiothreitol (DTT—reducing conditions) and the other without it. The insoluble/chromatin fraction was discarded as all proteins assayed for expression were present in the soluble/cytoplasmic fraction.

EVs, both total and CD81 + affinity-purified (AP), were lysed in EV-lysis buffer (1% NP-40, 5% glycerol, 0.5% sodium dodecyl sulfate, 0.5% sodium deoxycholate, 150 mM NaCl, and 1 mM PMSF). One fraction had 1 mM DTT, and the other did not. Both cell and EV fractions were run on 4-12% NuPAGE Bis-Tris 15-well gels (ThermoFisher NP0336BOX) using 1× Bolt MES buffer (ThermoFisher B0002) at 150 V for ∼60 min. A PageRuler Plus Prestained ladder (ThermoFisher 26619) was used to track protein migration. Proteins were transferred to a nitrocellulose membrane (Bio-Rad 1620115) at 250 mA for 90 min. Membranes were blocked with 8% milk in TBS-T for 30 min, and then, primary antibodies at dilutions, listed in Table S1, in 8% milk in TBS-T were incubated with the membrane for >1 h. Membranes were vigorously washed 3 times with TBS-T for 10 min per wash, and then, secondary antibodies at dilutions, listed in Table S1, in 8% milk in TBS-T were incubated with the membrane for >1 h. Images were taken on a Li-Cor Odyssey and analyzed using Image Studio V. 5.2. Tetraspanin proteins were detected using non-reducing conditions, whereas other proteins were detected in the presence of reducing conditions.

CFF of EVs and Precipitation

The cell culture supernatant or tumor fluid was initially passaged through a 0.22 μM PES vacuum filtration device (Olympus 25-227). The filtered fluid was adjusted—as needed—to 500 mL and added to the cross-flow filtration (CFF) chamber of an AKTA Flux (GE Healthcare 29038437). The solution was pushed through the system via peristalsis at a constant feed rate of 55 mL/min. A 750 kDa hollow-fiber cartridge filtration apparatus (GE Healthcare 29-0142-95) was used to exclude molecules smaller than vesicular bodies. A constant pressure feed (P_F) was set to 30 pounds per square inch (PSI), which kept the pressure retentate (P_R) between 10 and 15 PSI. The equilibration chamber was loaded with 500 mL of 1× PBS. A constant chamber volume of 50 g was set (with 1 mL = 1 g), which allowed for a 10× concentration of the initial solution and equilibration with 1× PBS (Gibco 14190-144). EVs were equilibrated in at least 200 mL of PBS before proceeding to the next step.

Total EVs were precipitated with the addition of 40 mg/mL PEG diluted in 1X PBS. EVs were precipitated out of solution at 4 °C for 24 h and then pelleted at 1,200×g at 4 °C for 30 min. The EV pellet was resuspended in 500 μL of 1× PBS. Non-EV-encased nucleic acid complexes were digested with the addition of 50 μg/mL RNaseA (Promega A7973) for 30 min at 37 °C. A full, extended protocol can be found in ref 15.

Fractionations and Drug-Loaded EV Sample Pooling

A concentration of 5×10^{12} EVs (either total EVs or CD81 + AP EVs) was diluted into 450 μL of fresh 1× PBS. Dimethyl sulfoxide (DMSO) was added to the EVs to a final concentration of 5% to facilitate drug solubility. Drugs were then incubated with purified EVs at 4 °C for 24 h with continuous rocking. Doxorubicin and paclitaxel Oregon Green 488 (Flutax-2, Invitrogen P22310) were added to a final concentration of 64 ng/μL. For non-specific membrane labels, the Vybrant CM Dil dye (ThermoFisher V22888) was added to a final concentration of 10 μM. After incubation, the EV mixtures were then loaded onto equilibrated Capto Core 700 HiTrap columns (GE Healthcare 17-5481-51). Fractions were collected using the AKTA Start (GE Healthcare 29022094-ECOMINSSW) into sterile 1.5 mL tubes. The settings used for fraction collection are outlined in Table S2.

Drug or membrane fluorophore (DiI or CellMask) EV fractions were identified using the BMG LabTech FluorStar Optima plate reader. Fractions were further validated for the presence of EVs using nanoparticle tracking analysis (NTA—see below). Fractions of high concentrations of EVs and fluorescence were pooled together.

Affinity-Purification of EVs

Anti-CD81 magnetic Dynabeads (ThermoFisher 10616D) were equilibrated in 1× PBS for a total of three washes. Total EVs (1×10^{11} to 1×10^{12}) were then added to the equilibrated and CD81 + EVs were allowed to bind to the beads at 4 °C for >2 h. Beads were then immobilized on a magnetic strip, and the flow through was collected. Beads were washed with cold 1× PBS for a total of three washes. The CD81 + EVs were eluted from the beads in a total volume of 100 μL of 0.2 M glycine (pH = 2.0, filtered through a 0.22 μm membrane) at 37 °C for 10 min. The acidic glycine was neutralized through the addition of 100 μL of neutralization buffer (100 mM Tris-HCl pH = 7.5, 1× PBS).

Flow Cytometry

EVs were bound to magnetic anti-CD81 beads (ThermoFisher 10616D) and washed to remove unbound material as described in the previous section. The bead slurry was analyzed by flow cytometry using the BD Accuri 6 Plus flow cytometer (BD Biosciences, 23-17667-00) equipped with 488 and 640 lasers, along with the emission filters FITC (519 nm), PE (578 nm), PerCP (678 nm), and APC (660 nm). The instrument was calibrated using CS&T beads (Fisher 661414). A

https://doi.org/10.1021/acsbiomedchemau.1c00030
ACS Bio Med Chem Au 2022, 2, 140−149

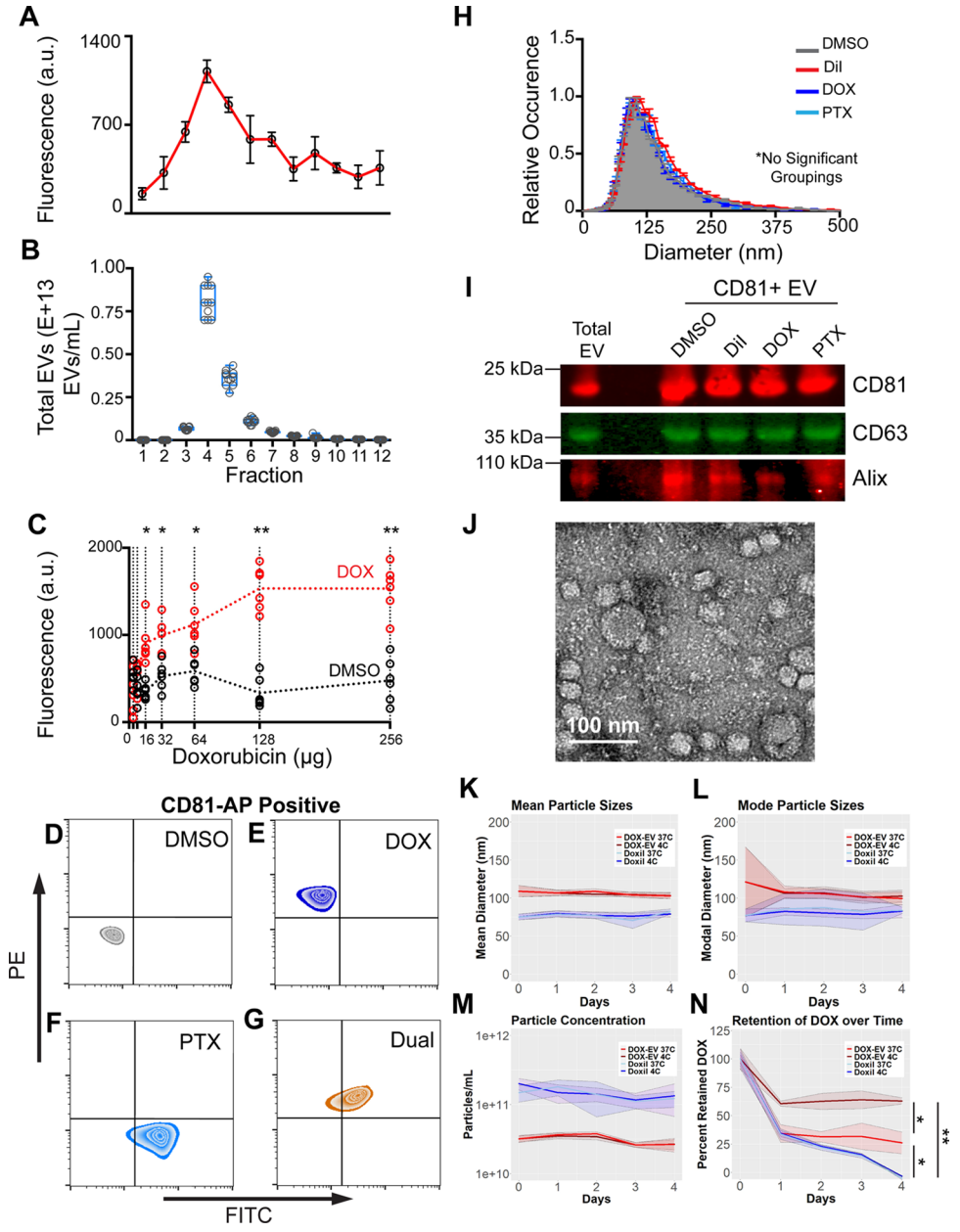

Figure 1. Generation of drug-loaded KSHV-EVs. (A) Total EVs were labeled with the non-specific membrane intercalating dye DiI and fractionated using Capto Core 700 resin; fluorescence (*y*-axis) was quantified of each fraction (*x*-axis). (B) Total EV concentration (*y*-axis) from Capto Core fractions (*x*-axis) was measured by nanoparticle tracking analysis. (C) Increasing concentrations of doxorubicin (*x*-axis) were incubated with total EVs and then filtered through Capto Core 700 resin. EV positive fractions were identified as in A and B, pooled, and compared to similar fractions of mock-loaded EVs. Fluorescence as a measure of the DOX content is shown on the vertical axis, and the concentration of DOX in the loading buffer is shown on the *x*-axis. (D−G) Flow cytometry analysis of CD81 + AP EVs (post fractionation, immobilized on beads) loaded with either (D) DMSO, (E) DOX (fluorescent in the PE channel, *y*-axis), (F) paclitaxel Oregon Green 488 (fluorescent in the FITC channel, *x*-axis), or (G) both. (H) Size distribution analysis of eluted CD81 + EVs with the diameter size (*x*-axis) and relative occurrence (*y*-axis) plotted. (I) Immunoblot analysis of protein markers in the total EVs and CD81 + EVs. (J) Representative TEM micrograph of CD81 + EVs. (K) Mean particle sizes of DOX-KSHV-EVs and Doxil that were incubated at 4 and 37 °C, and the non-retained drug was removed via Capto Core 700 at 24 h intervals. (L) Same as A but modal particle sizes. (M) Particle concentration of DOX-KSHV-EVs and Doxil at the indicated times and temperatures. (N) Percent drug retention in DOX-KSHV-EVs and Doxil over 4 days at 4 and 37 °C; input fractions are at day 0, and the drug concentration for each group was arbitrarily set to 100% ($n = 3$ for each group, shown are mean values ± SD for each time point; ANOVA was done to determine statistical groupings) * = $p < 0.05$, ** = $p < 0.01$ where indicated.

total of >50,000 beads were analyzed for fluorescence intensity. Data were plotted and analyzed using FlowJo v 10.0 using contour plots.

EV Quantitation and Biophysical Characterizations

Size-distribution profiles, concentrations, and zeta potential of EVs and drug-infused vesicles were performed using the ZetaView from Particle Metrix. NTA was standardized using manufacturer-supplied 102 nm polystyrene beads (zeta potential and size) and house-made EV concentration standards (standard = 1×10^{13} particles/mL).

Solutions were diluted in nanopure water until approximately 50−200 particles were present per field of view. Size-distribution profiles and concentrations were taken using 11 technical replicates per sample; zeta potential measurements were taken using five technical replicates

https://doi.org/10.1021/acsbiomedchemau.1c00030
ACS Bio Med Chem Au 2022, 2, 140−149

per sample. A total of ≥ 5 biological replicates per treatment were done to ensure reproducibility. Statistical groupings were done using ANOVA followed by pairwise *t*-tests ($p < 0.05$).

Treatment of Cells with Drug-Loaded EVs and Liposome-Encapsulated Drugs

EVs with DMSO or drug or liposome chemotherapy drugs were quantified using NTA for concentration. As an adsorption control, cells were treated with Dil-labeled EVs to ensure the transfer of the fluorophore from EVs to a recipient cell. Cells were then treated with drugs and quantified for DNA damage using indirect immunofluorescence and cell growth via xCelligence proliferation assay (see below).

Fluorescence and Indirect Immunofluorescence Microscopy

The EV-labeled Vybrant CM DiI dye was diluted to a concentration of 10 μM in the EV slurry before Capto Core filtration. DAPI was diluted to 100 ng/mL in water to stain the nucleus immediately before mounting. Alexfluor-488 phalloidin (Invitrogen A12379) and Alexfluor-647 phalloidin (Invitrogen A22287) were used to stain intracellular actin filaments.

For indirect immunofluorescence, primary antibodies were diluted in 10% bovine serum albumin (BSA) (Fisher) in 1× PBS. Cells were fixed in 4% paraformaldehyde and permeabilized in 0.1% Triton X-100 diluted in PBS. Primary antibodies were diluted at concentrations shown in Table S1 and incubated with the permeabilized cells for 1 h at room temperature in a humidity chamber. Slides were washed three times in 1× PBS and incubated with secondary antibodies (diluted in 10% BSA) at room temperature for 1 h. After final washes and incubations, slides were mounted onto frosted micro slides (Corning 2948-75 × 25) using a Molecular Probes ProLong Gold antifade reagent (Cell Signaling 9071S). Images were taken using a Leica DM5500 upright widefield fluorescence microscope (Leica Microsystems, Wetzlar, Germany) using either an HCX PL apochromatic 63× oil objective lens with a numerical aperture (NA) of 1.40−0.60 or an HCX PL apochromatic 100× oil objective lens with a 1.40−0.70 NA. Images were acquired using a Retiga R3 2.8-megapixel CCD digital microscope camera (Teledyne QImaging, Surrey, BC, Canada). Z-stacks were captured and deconvoluted using MetaMorph V 7.8.12.0 (Molecular Devices) software and visualized using Imaris V 9.2.0 (Bitplane).

Doxorubicin Retention Assay

KSHV-EVs from BCBL-1 cells were purified as described above and incubated with doxorubicin overnight at 4 °C. Excess/unincorporated doxorubicin was removed through Capto Core 700 filtration. The initial drug concentration and EV quantitation were done on the DOX-KSHV-EVs, as was Doxil. DOX-KSHV-EVs and Doxil were then aliquoted into 5 individual tubes of 200 μL and placed at 4 °C or 37 °C for 24 h. Single tubes were removed and mixed with 50 μL of Capto Core 700 slurry to remove the unincorporated drug. The slurry was pelleted, and DOX-KSHV-EV and Doxil (upper aqueous layer) were removed and stored at −80 °C. The process was repeated for a total of five measurements (one at $T = 0$ and four for the four days post-initial Capto Core 700 filtration) using the individually aliquoted tubes.

The concentration of EVs in the DOX-KSHV-EVs or liposomes in Doxil was quantified using the ZetaView at each time interval, as were the mean and mode sizes. The drug concentration was calculated by fluorometric assay on the Tecan Infinite M200 Pro plate reader (Tecan 30016056). A total volume of 50 μL per well was added to a round bottom 96-well plate. Fluorescence readings of the solutions were quantified using an excitation wavelength of 500 nm and an emission filter of 595 nm, in line with known fluorescence properties of DOX.[16] A standard curve was made using known concentrations of DOX to calculate the amount of the drug retained in the DOX-KSHV-EVs and Doxil over time.

Cell Proliferation Assay

Cell proliferation indexes were determined using the xCELLigence E-plate 16 (Acea Biosciences). A total of 20,000 cells/well of hTERT-HUVECs were treated with PBS (negative control), CD81 + KSHV-EVs (positive control, DiI-labeled), Doxo-CD81 + KSHV-EVs, or equivalent particles/mL (1E + 10) of Doxil. Cells were allowed to grow for >40 h, and cell index reads were taken every 5 min. Statistically significant groupings were determined by ANOVA followed by Tukey−Kramer tests.

Mouse Injections

Athymic nude mice (NU/J) originally obtained from Jackson Laboratories (Bar Harbor, ME) were maintained by the UNC Animal Studies Core. Five male and five female mice were used per study group per experiment. Mice were given subcutaneous unilateral flank injections of EVs diluted in an equal volume of Matrigel to a total volume of 0.5 mL. The location of the injection site was chosen for minimal interference with ambulation and normal activities. All mice were maintained under pathogen-free conditions using microisolator cages and monitored during the 7 day experimental period for body condition, weight, malaise, and motility issues. Animals were classified and approved under USDA Pain and Distress Category C: "slight or momentary pain or distress or no pain or distress" by the UNC Institutional Animal Care and Use Committee (IACUC).

Mice were to be euthanized at a humane endpoint defined as displaying malaise, having a body score equal to or less than 2, or reaching 7 days post-injection, whichever came first. Animals experiencing unrelieved pain or distress before the endpoint, as defined by institutional policy, must be humanely euthanized unless an exception to policy is requested and approved. No exception to this policy was requested or granted. No mice died or reached an approved endpoint during the 7 days and were therefore euthanized on day 7 via a controlled-flow carbon dioxide chamber followed by approved secondary cervical dislocation. Select mice were injected via the lateral tail vein with 100 μL of Evan's Blue (EB) dye 1% v/v in sterile PBS 30 min before euthanasia so that the tissue vasculature could be macroscopically imaged after removal. These EB-containing tissues were not used for immunofluorescent studies. Immediately after euthanasia, tissues were collected in 10% neutral buffered formalin and fixed at 4 °C for 48 h before processing and sectioning.

RESULTS

Total EVs from PEL cells were isolated as previously described[15] and detailed in Methods. A summary of the workflow is depicted in Figure S1. EV purity and concentration were ascertained by nanoparticle tracking analysis (Figure 1A,B). The EVs were loaded with either doxorubicin (DOX) or mock-treated (Figure 1C) by mixing at a physiological pH. As DOX is naturally fluorescent, dose-dependent loading of EVs was ascertained by ELISA. Similar experiments were performed with PTX, using a tagged paclitaxel Oregon Green-488 derivative (Figure S2). Unlike the loading of artificial liposomes or other nanoparticles, EV loading was possible without force, breaking, or re-assembling as DOX and PTX naturally partitioned into and, more importantly, through lipid membranes while both components were being mixed. As no external force was used, the biological integrity of the EVs was maintained.

The drug-loaded EVs were affinity purified and immobilized using anti-CD81 beads as described,[3,17,18] which removed any unincorporated drug. The immobilized EVs retained both drugs as ascertained by three-color flow cytometry on the anti-CD81 beads (see Figures 1D−G and S2). CD81-AP was used as a marker for EVs, DOX was measured in the PE channel, and PTX Oregon Green-488 was measured in the FITC channel. It was possible to generate EVs that contained both drugs as indicated by the shift in the population into the upper right quadrant (Figure 1D). The ability to uptake and retain these compounds was also observed in EVs from primary patient tumor effusion fluid or plasma from healthy donors (Figure S3), which suggests that this approach may be suitable for personalized therapy.

https://doi.org/10.1021/acsbiomedchemau.1c00030
ACS Bio Med Chem Au 2022, 2, 140−149

To verify the composition and integrity of the drug-loaded EVs, the standard repertoire of EV quality-control measurements[19] were conducted. Drug uptake did not affect the EV size as measured by nanoparticle tracking analysis (NTA) (Figure 1H). Shifts in zeta potential were observed (Figure S4), consistent with previous observations.[20,21] This can be attributed to a fraction of the drugs being intercalated into the membrane of the EV or on the EV surface, in addition to a fraction encased (see below). The EV protein composition remained unaffected by drug incorporation as measured using Western blot for known markers CD81, CD63, and Alix (Figure 1I). The EVs were observed under transmission electron microscopy (TEM), revealing a sphere-like morphology and membrane flexibility (Figures 1J and S5). The EV-encased miRNAs remained readily detectable, and the signal was RNase-resistant, demonstrating that the miRNAs were localized inside and that the EVs remained physically intact throughout all experimental manipulations (Figure S6). Intracellular miRNA-, pre-miRNA-, and other miRNA-precursor concentrations were higher than those in the EV fraction.[12]

To compare retention of the drug over time, a temporal retention assay was performed at 4 °C and 37 °C. Unincorporated DOX from DOX-KSHV-EVs or Doxil was removed every 24 h (see Methods). Although particle sizes and concentrations remained mostly constant (Figure 1K−M), DOX-KSHV-EVs stored at 4 °C had significantly higher retention of the drug than Doxil at 4 °C and likewise for DOX-KSHV-EVs at 37 °C. Interestingly, the rate of DOX leakage from Doxil did not appear to be affected by temperature but the temperature did affect the leakage rate in DOX-KSHV-EVs (Figure 1N).

The drug-loaded EVs were fusion-competent in endothelial cells (ECs), which are the targets of transformation by KSHV (Figures S7 and S8). ECs are the lineage of origin for KS. They are crucial in providing a microenvironment for the distant metastasis of any tumor, and EC reprogramming is essential for neoangiogenesis. As reported previously, tumor-derived KSHV-EVs dramatically enhance the proliferation and migration of normal ECs.[6,12,13] To determine if DOX-loaded KSHV-EVs were able to reduce the viability of cells where they originated from, mock- or DOX-loaded EVs were added to target cells and assayed for DNA damage by immune fluorescence using phospho-histone gammaH2A.X accumulation as a marker for DNA damage (Figure 2A−L). This is an endpoint assay. Upon exposure to DOX-EVs, but not to mock-loaded EVs, phospho-gammaH2A.X was readily detectable at 24 h post-incubation. Liposomal doxorubicin (Doxil) and the free doxorubicin were used as positive controls. Similar results were obtained with PTX-loaded KSHV-EVs (Figure S9). This demonstrated that drug-loaded KSHV-EVs functionally delivered their payload at least as effectively as the free drug or the liposome-encapsulated drug that is the current clinical standard of care.

To quantitate the potency of the effect, real-time measurements of cell growth over time (xCelligence system) were used as an orthogonal assay. This enabled a quantitative comparison as the same number of DOX-loaded KSHV-EVs and commercial liposomal doxorubicin was used as input. DOX-loaded KSHV-EVs inhibited cell growth earlier and in more cells than liposomal doxorubicin (Figure 2M). The differences in the rate could be due to the following reasons: (i) an increased concentration of DOX delivered by KSHV-EVs relative to Doxil, (ii) faster uptake of EVs relative to Doxil, (iii) shuttling of the DOX via nucleic acids directly to the nucleus, or (iv) a combination of some or all of the above.

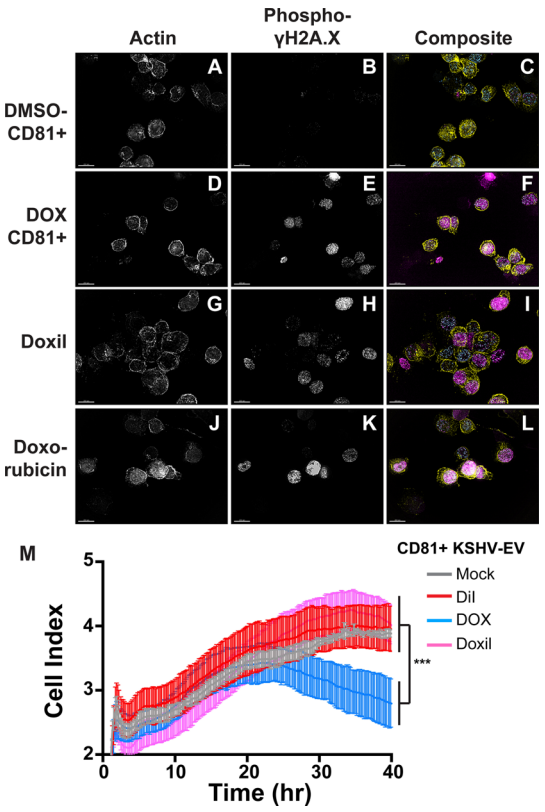

Figure 2. Drug-loaded KSHV-EVs are functional. CD81 + AP KSHV-EVs were isolated from PEL, drug-loaded or mock (DMSO)-treated, and added to target¬ cells; (A−C) mock-loaded EVs, (D−F) DOX-EVs; (G−I) Doxil, (J−L) or doxorubicin alone. Stains are for actin, phospho-γH2A.X, and composite. All images at 100× magnification. (M) Growth of endothelial cells treated with indicated treatments; the horizontal axis is time, and the vertical axis is the cell growth index.

To investigate these phenotypes *in vivo*, mock-loaded EVs and DOX-EVs were mixed with Matrigel and implanted subcutaneously into mice. Matrigel containing PBS was used as the negative control, and Matrigel containing vascular endothelial growth factor (VEGF) was used as the control for the recruitment and differentiation of CD34 + cells. This assay allowed us to estimate local distribution and, more importantly, the effect on neoangiogenesis due to ECs infiltrating the Matrigel plug. The fluorescent membrane dye DiI was used to track the mock-loaded EVs. Injection sites, which were on the rear, right hip, were still highly fluorescent 72 h after the implant in the mock- and DOX-EVs (DOX itself is weakly fluorescent and therefore tractable) (Figures 3A−D, S10−S11). A fraction dispersed from the site of injection and circulated systemically. As expected, only a background signal was observed in the PBS- or VEGF-mixed Matrigel implants, as those were not fluorescent.

Both VEGF and KSHV lymphoma EVs stimulate EC migration and neoangiogenesis.[12,13] In fact, VEGF (and PDGF) has been recognized as the driving factor in KS angiogenesis.[22] Histology showed that ECs were recruited into the VEGF- and KSHV-EV-loaded Matrigel plugs but not into the PBS Matrigel plug (Figure 3E,H,K). The invading ECs were CD34 positive (Figure S11). KSHV-EVs were more potent than VEGF with regard to neoangiogenesis. Fluorescent measure-

https://doi.org/10.1021/acsbiomedchemau.1c00030
ACS Bio Med Chem Au 2022, 2, 140−149

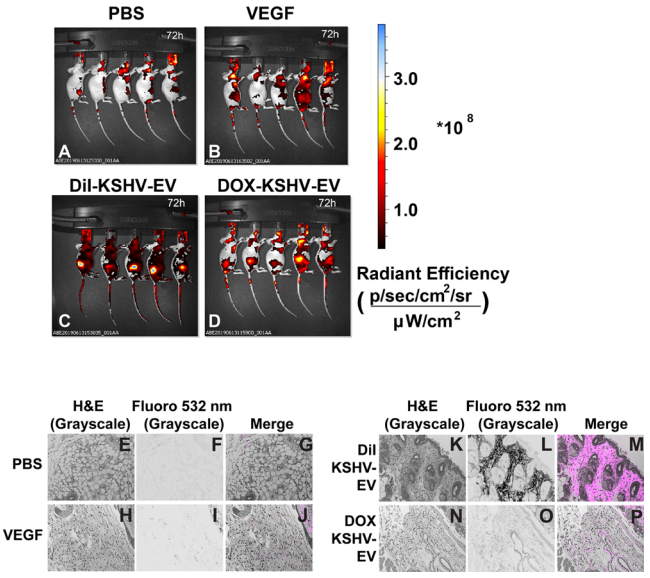

Figure 3. DOX-KSHV-EVs inhibit neoangiogenesis. (A–D) Athymic nude mice (both male and female) were administered Matrigel plugs subcutaneously that were loaded with (A) PBS, (B) VEGF, (C) DiI-KSHV-EVs, or (D) DOX-KSHV-EVs. The EVs were affinity purified using CD81-antibody-coated beads prior to administration. The mice were monitored for adverse reactions and briefly anesthetized to scan for fluorescence 72 h after injection. (E–P) Histology in the Matrigel plug using H&E staining and fluorescence (excitation = 532 nm, measuring DiI) of mice treated with (E–G) PBS, (H–J) VEGF, (K–M) DiIKSHV-EVs, and (N–P) DOX-KSHV-EVs; images at 40× magnification. All tissue slices were taken at 7 days post injection. Fluorescence signals above the background were colored pink for contrast. DOX is weakly fluorescent over the background, and the pink signal in the DOX-KSHV-EVs was likely remnant DOX.

ments of the DiI tracking dye showed that KSHV-EVs were taken up by the invading EC (Figure 3L). DOX-KSHV-EVs were also taken up by arriving ECs that suppressed their neoangiogenesis (Figure 3O,L); in contrast to intact endothelial sprouting vasculature, apoptotic debris accumulated in the DOX-KSHV-EV plugs (Figure S12). As both mock- and DOX-KSHV-EVs are derived from the same tumor, they have the same composition of proteins and RNAs. Therefore, the incorporation of chemotherapy compounds converted their pro-tumor phenotype into an effective anti-tumor and anti-angiogenesis phenotype.

To test the hypothesis that the miRNA cargo in EVs was the reason for higher drug retention in EVs as compared to artificial liposomes, DICER KO cells were used to generate miRNA-free EVs (Figure S13). Figure 4A shows that DICER was deleted in the producer cell lines and that this had no effect on EV marker composition. The DICER KO cells produced EVs at a similar magnitude and with similar biophysical properties as the control (Figure S14). The miRNA-free EVs incorporated significantly less DOX than miRNA-positive EV controls as measured by flow cytometry (Figure 4B,C). This was not the case for the long chain dialkylcarbocyanine dye DiI, which has been historically used to stain the plasma membrane of cells[23] and which we have previously used to stain EVs[24] (Figure S15). Moreover, the DOX-EVs contained twice as much doxorubicin per particle as Doxil (Figure 4D) as determined by mass spectrometry using a clinical assay for the detection of doxorubicin.[25] These results were consistent across ≥ 3 independent lots of EV-Dox attesting to the robustness and reproducibility of this method.

The proposed mechanism of action stipulates that EV-encased miRNAs were acting as sponges for nucleic acid intercalating drugs such as DOX and that this led to higher drug concentrations compared to artificial liposomes that consist only of a lipid shell. To further test this model, a competition experiment was performed. Doxil [a formulation of doxorubicin in *N*-(carbonyl-methoxy polyethylene glycol 2000)-1,2-distearoyl-*sn*-glycerol-3-phosphoethanolamine, phosphatidylcholine, and cholesterol liposomes] was mixed with EVs, and the amount of doxorubicin transferred into CD63-GFP positive EVs was measured over time using flow cytometry (Figure 4E,F). The drug was readily transferred from the artificial liposomes into the natural EVs. This was possible because in Doxil, the liposomal formulation of DOX, the drug exists in an equilibrium between the free drug and liposome-associated drug. The EVs can capture the free drug and retain it when mixed with Doxil. In fact, DOX leakage during storage and liposomal instability is a limitation to the clinical use of Doxil and the root cause for some of the Doxil-associated toxicity. Drug transfer was not a result of membrane fusion or envelopment of Doxil liposomes by EVs as ascertained by size measurements (Figure S16).

These results demonstrate that in a direct competition experiment between a purely lipid particle and an EV, doxorubicin will be preferentially partitioned into miRNA-positive EVs.

DISCUSSION

Metastasis, rather than the growth of the primary tumor, drives mortality for most cancers. Neoangiogenesis and extravasation of the primary tumor cell into the circulation are essential for metastasis. KS, next to hemangioma, is the most angiogenic tumor in humans (reviewed in ref 11) and thus serves as a relevant model to explore novel drugs and delivery modes for cancer. Paracrine effects on both the local microenvironment and distant sites are central to KS and to metastasis in general. EVs have been shown to be potent mediators of the paracrine effects in KS, and in general, tumor-derived EVs show tissue selectivity, where they prepare the microenvironment, mostly ECs ("the soil"), to support subsequent tumor cells ("the seed"), a hypothesis first proposed by Folkman.[26] In sum, tumor-derived EVs reprogram and attract EC cells to create a pro-tumor microenvironment and prime distant sites for metastasis.[6,9,12,13]

This report shows that EVs could be loaded with chemotherapeutic compounds as easily as artificial liposomes, that this process does not affect EV biology or integrity, and that the resulting therapeutic EV formulation had superior anti-tumor activity in culture and anti-angiogenesis activity *in vivo*. The drug concentration in DOX-EVs was twice that of Doxil, the current first-line clinical treatment for KS.

The reason for the higher drug-loading capacity of the EV was the presence of miRNAs in EVs and perhaps other cargo and a more complex lipid composition that facilitates drug uptake and higher retention rates.[27−30] This suggests that adding nucleic acids to artificial lipid formulations may be similarly effective in increasing drug formulation. It would, however, lack the tumor-derived EVs intrinsic tissue targeting properties.[9,12,13,31,32] At this point, there is no evidence that the viral miRNAs had a specific effect. In our system, EVs derived from the KSHV-driven tumor would be superior to artificial liposomes in delivering doxorubicin, paclitaxel, or other compounds that bind to RNA.

https://doi.org/10.1021/acsbiomedchemau.1c00030
ACS Bio Med Chem Au 2022, 2, 140−149

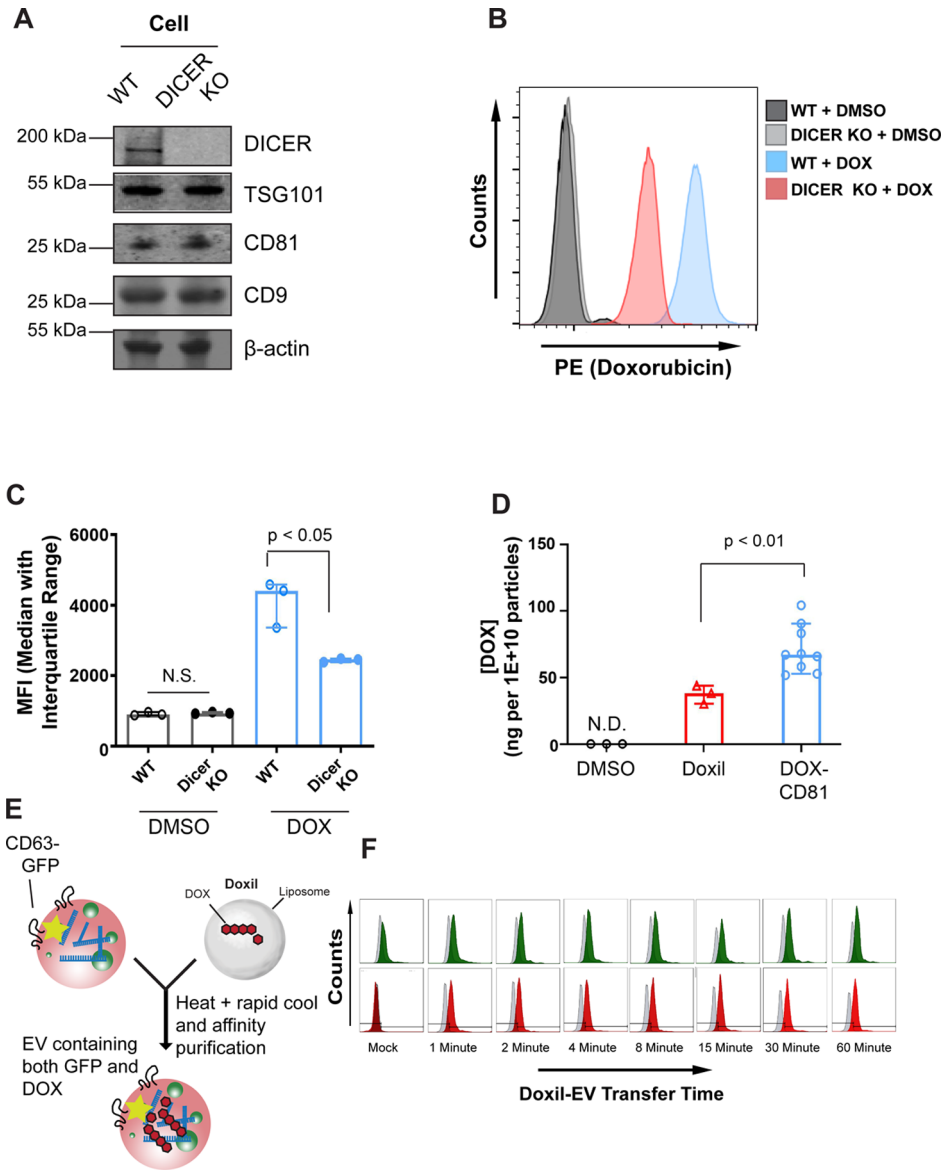

Figure 4. EV-encased miRNAs increase drug loading. (A) Immunoblot panel of WT and Talon-mediated DICER KO HEK 293T cells. (B) Flow cytometry histograms of CD81 + EVs loaded with DMSO or DOX from WT or DICER KO cells; the *x*-axis is DOX fluorescence, and the *y*-axis is count incidence. (C) Mean fluorescence intensity (MFI) of CD81 + EVs immobilized on beads analyzed in B, open circles are WT, and closed circles are DICER KO. (D) Mass spectrometry quantitation of total [DOX] per 1E + 10 particles (*y*-axis) between Doxil and DOX-KSHV-EVs (*x*-axis); DMSO loaded KSHV-EVs are shown as the control and did not have detectable DOX. (E) *In vitro* transfer of DOX between CD63-GFP EVs and Doxil. The CD63 was tagged with a GFP to allow for flow cytometry gating on fluorescently positive beads. (F) After EV and Doxil were mixed for the indicated times, the EVs were immobilized on CD81 + beads and analyzed by flow cytometry for GFP (top) and subsequently for DOX (bottom) fluorescence intensities (*x*-axis) as a function of time of incubation.

Uncoupling of drugs from nucleic acid sponges upon delivery through EVs clearly occurs, although the metabolism of delivered EV contents through the endosomal recycling pathway remains an emerging field, and sorting mechanisms are still being deduced. It is important to note that our study used naturally occurring and unmodified nucleic acids as carriers. Previous work has shown that chemical modifications to RNA nucleotides, artificial caps, and 3′ modifications can reduce degradation, particularly by pattern recognition receptors in the endosomal-trafficking network. Our results support a model of rapid dissociation of nucleic acid-interacting drug, in line with degradation of the nucleic acid. We acknowledge that a caveat to this study is that the EVs used were from a KSHV-driven malignancy, which contains unusually high concentrations of miRNAs mostly of viral origin. We were nonetheless surprised to find that EV-delivered DOX decreased proliferation more than Doxil or doxorubicin (Figure 2). This could be due to the following reasons: (i) an increased concentration of DOX delivered by EVs relative to Doxil, (ii) faster uptake of EVs relative to Doxil or the drug alone, (iii) direct shuttling of DOX to the nucleus by EV-encased nucleic acids, or (iv) a combination of all of the above. We cannot discount that nucleic acids other than miRNAs also play a role in DOX uptake and retention. Further studies using EVs that naturally contain fewer miRNAs, or the addition of nucleic acids with stabilizing modifications, are warranted.

Tissue targeting of EVs has been of high interest, particularly as it relates to cancer metastasis (reviewed in ref 33). We

https://doi.org/10.1021/acsbiomedchemau.1c00030
ACS Bio Med Chem Au 2022, 2, 140−149

previously showed that KSHV-EVs are readily uptaken by endothelial cells, the target of transformation in KS, and transcriptionally reprogram the cells.[13] Others have identified tissue targeting by EVs and have linked it to surface receptors such as integrin β1 and gangliosides.[34,35] Although we identified a strong tissue preference for CD34+ endothelial cells for KSHV-EVs, we cannot discount that a fraction went elsewhere.

This study has several limitations. For example, drug loading into PEL EVs and plasma EVs is not an exact comparison. All EVs can carry miRNAs, but only in EVs from PEL are KSHV miRNAs present. Figure S3 shows that the origin of the EVs does not affect loading; however, one cannot attribute drug retention exclusively to miRNAs. Other species of RNA have been reported inside EVs that can coordinate nucleic acid-binding chemotherapy agents. DICER depletion would not affect their levels. Shifts in zeta potential upon drug loading signify that not all the loaded chemotherapy agents are inside the EV. Although we propose that encased nucleic acids play a role in drug-retention, particularly those that are membrane-permeable, we cannot discount that a fraction of drug would be associated with EVs independent of nucleic acids, presumably in the membrane.

How would these results be translated into clinical practice? Off-target cardiac toxicity limits the use of doxorubicin. Encasing doxorubicin into liposomes dramatically reduced the off-target toxicity of the soluble drug. This led to the FDA approval of Doxil. Similarly, Abraxane represents an approach to formulate paclitaxel to increase the half-life and reduce toxicity of the free drug. EVs represent an alternative approach, with a higher payload and the prospect of biologically determined tissue specificity.

About 10^{11} EVs/mL circulate in human plasma[36] and are as easily purified as platelets. Unlike cells, EVs do not induce allogeneic rejection. In fact, with each routine transfusion, many more EVs are transduced than platelets across HLA-mismatched individuals. Hence, DOX-loaded EVs can be stored and used as an off-the-shelf product. For Doxil, where the liposomes are also pegylated to improve the half-life *in vivo*, anaphylactic reactions have been reported for ~25% of cases, and repeat injections are associated with the development of an anti-PEG antibody response (reviewed in ref 37). This can lead to accelerated blood clearance of repeat Doxil infusions as needed for KS treatment.

An alternative scenario uses EVs isolated from a patient's primary tumor, loaded with chemotherapy drugs *ex vivo*, and reinfused to prevent metastasis through this "poisoning the soil" approach. As each tumor type extrudes different EVs, this approach can be thought of as a form of personalized therapy.

Study Approval

All applicable international, national, and institutional guidelines for the care and use of animals were followed, and all procedures performed in studies involving mice followed the ethical standards of UNC IACUC. Experiments were approved under IACUC protocol number 17-204.0. Personnel interactions with mice were registered by animal handlers certified in mouse handling and techniques by the UNC Office of Care and Animal Use in compliance with the U.S. federal law.

ASSOCIATED CONTENT

Supporting Information

The Supporting Information is available free of charge at https://pubs.acs.org/doi/10.1021/acsbiomedchemau.1c00030.

List of antibodies, manufacturing origin, purpose, and dilutions, list of settings used during total EV purification and fractionation on the AKTA start, and supplementary figures and their corresponding captions (PDF)

AUTHOR INFORMATION

Corresponding Author

Dirk P. Dittmer − *Lineberger Comprehensive Cancer Center and Department of Microbiology and Immunology, The University of North Carolina at Chapel Hill School of Medicine, Chapel Hill, North Carolina 27599-9500, United States*; orcid.org/0000-0003-4968-5656; Email: ddittmer@med.unc.edu

Authors

Ryan P. McNamara − *Lineberger Comprehensive Cancer Center and Department of Microbiology and Immunology, The University of North Carolina at Chapel Hill School of Medicine, Chapel Hill, North Carolina 27599-9500, United States*

Anthony B. Eason − *Lineberger Comprehensive Cancer Center and Department of Microbiology and Immunology, The University of North Carolina at Chapel Hill School of Medicine, Chapel Hill, North Carolina 27599-9500, United States*

Yijun Zhou − *Lineberger Comprehensive Cancer Center and Department of Microbiology and Immunology, The University of North Carolina at Chapel Hill School of Medicine, Chapel Hill, North Carolina 27599-9500, United States*

Rachele Bigi − *Lineberger Comprehensive Cancer Center and Department of Microbiology and Immunology, The University of North Carolina at Chapel Hill School of Medicine, Chapel Hill, North Carolina 27599-9500, United States*

Jack D. Griffith − *Lineberger Comprehensive Cancer Center and Department of Microbiology and Immunology, The University of North Carolina at Chapel Hill School of Medicine, Chapel Hill, North Carolina 27599-9500, United States*

Lindsey M. Costantini − *Lineberger Comprehensive Cancer Center and Department of Microbiology and Immunology, The University of North Carolina at Chapel Hill School of Medicine, Chapel Hill, North Carolina 27599-9500, United States; Department of Biological and Biomedical Sciences, North Carolina Central University, Durham, North Carolina 27707, United States*

Michelle A. Rudek − *Sidney Kimmel Comprehensive Cancer Center, Johns Hopkins School of Medicine, Baltimore, Maryland 21205, United States*

Nicole M. Anders − *Sidney Kimmel Comprehensive Cancer Center, Johns Hopkins School of Medicine, Baltimore, Maryland 21205, United States*

Blossom A. Damania − *Lineberger Comprehensive Cancer Center and Department of Microbiology and Immunology, The University of North Carolina at Chapel Hill School of Medicine, Chapel Hill, North Carolina 27599-9500, United States*

Complete contact information is available at: https://pubs.acs.org/10.1021/acsbiomedchemau.1c00030

Author Contributions

R.P.M and D.P.D. conceptualized, curated, and analyzed the experiments. R.P.M, A.B.E., L.M.C., R.B., Y.Z., J.D.G., B.A.D., M.A.R., N.M.A., and D.P.D developed the methodology and

https://doi.org/10.1021/acsbiomedchemau.1c00030
ACS Bio Med Chem Au 2022, 2, 140−149

investigated and administered aspects of this project. R.P.M, B.A.D., J.D.G, and D.P.D. provided supervision and validation and wrote the article. Funding was provided by R.P.M., J.D.G., L.M.C., B.A.D., and D.P.D. Data and material availability: All data are available in the main text or the Supporting Information.

Notes

The authors declare no competing financial interest.

■ ACKNOWLEDGMENTS

We thank Brian Cullen for DICER-deleted HEK-293 cells. This work was funded by the 5UM1CA121947-10 to R.P.M., the 1R01DA040394 to D.P.D., and the 2P01CA01901438 to J.D.G and B.A.D. The UNC Animal Studies Core and the UNC Flow Cytometry Core are supported by the NCI Center Core Support Grant (P30CA16086). The Analytical Pharmacology Shared Resource of the Sidney Kimmel Comprehensive Cancer Center at Johns Hopkins directed by M.A.R. is supported by the P30CA006973 and the UL1TR003098 and the Shared Instruments Grant S10RR026824. The project described was also supported by UL1TR003098 from the National Center for Advancing Translational Sciences (NCATS). Its contents are solely the responsibility of the authors and do not necessarily represent the official view of NCATS or NIH.

■ REFERENCES

(1) Tkach, M.; Théry, C. Communication by Extracellular Vesicles: Where We Are and Where We Need to Go. *Cell* **2016**, *164*, 1226−1232.
(2) Raab-Traub, N.; Dittmer, D. P. Viral effects on the content and function of extracellular vesicles. *Nat. Rev. Microbiol.* **2017**, *15*, 559−572.
(3) Pegtel, D. M.; Gould, S. J. Exosomes. *Annu. Rev. Biochem.* **2019**, *88*, 487−514.
(4) Mathieu, M.; Martin-Jaular, L.; Lavieu, G.; Théry, C. Specificities of secretion and uptake of exosomes and other extracellular vesicles for cell-to-cell communication. *Nat. Cell Biol.* **2019**, *21*, 9−17.
(5) Chevillet, J. R.; Kang, Q.; Ruf, I. K.; Briggs, H. A.; Vojtech, L. N.; Hughes, S. M.; Cheng, H. H.; Arroyo, J. D.; Meredith, E. K.; Gallichotte, E. N.; Pogosova-Agadjanyan, E. L.; Morrissey, C.; Stirewalt, D. L.; Hladik, F.; Yu, E. Y.; Higano, C. S.; Tewari, M. Quantitative and stoichiometric analysis of the microRNA content of exosomes. *Proc. Natl. Acad. Sci. U. S. A.* **2014**, *111*, 14888−14893.
(6) Yogev, O.; Henderson, S.; Hayes, M. J.; Marelli, S. S.; Ofir-Birin, Y.; Regev-Rudzki, N.; Herrero, J.; Enver, T. Herpesviruses shape tumour microenvironment through exosomal transfer of viral microRNAs. *PLoS Pathog.* **2017**, *13*, No. e1006524.
(7) Higuchi, H.; Yamakawa, N.; Imadome, K.-I.; Yahata, T.; Kotaki, R.; Ogata, J.; Kakizaki, M.; Fujita, K.; Lu, J.; Yokoyama, K.; Okuyama, K.; Sato, A.; Takamatsu, M.; Kurosaki, N.; Alba, S. M.; Azhim, A.; Horie, R.; Watanabe, T.; Kitamura, T.; Ando, K.; Kashiwagi, T.; Matsui, T.; Okamoto, A.; Handa, H.; Kuroda, M.; Nakamura, N.; Kotani, A. Role of exosomes as a proinflammatory mediator in the development of EBV-associated lymphoma. *Blood* **2018**, *131*, 2552−2567.
(8) Pegtel, D. M.; Cosmopoulos, K.; Thorley-Lawson, D. A.; van Eijndhoven, M. A. J.; Hopmans, E. S.; Lindenberg, J. L.; de Gruijl, T. D.; Middeldorp, J. M. Functional delivery of viral miRNAs via exosomes. *Proc. Natl. Acad. Sci. U. S. A.* **2010**, *107*, 6328−6333.
(9) Wortzel, I.; Dror, S.; Kenific, C. M.; Lyden, D. Exosome-Mediated Metastasis: Communication from a Distance. *Dev. Cell* **2019**, *49*, 347−360.
(10) Krishna, A. G.; Kumar, D. V.; Khan, B. M.; Rawal, S. K.; Ganesh, K. N. Taxol-DNA interactions: fluorescence and CD studies of DNA groove binding properties of taxol. *Biochim. Biophys. Acta* **1998**, *1381*, 104−112.
(11) Dittmer, D. P.; Damania, B. Kaposi sarcoma-associated herpesvirus: immunobiology, oncogenesis, and therapy. *J. Clin. Invest.* **2016**, *126*, 3165−3175.
(12) Chugh, P. E.; Sin, S.-H.; Ozgur, S.; Henry, D. H.; Menezes, P.; Griffith, J.; Eron, J. J.; Damania, B.; Dittmer, D. P. Systemically circulating viral and tumor-derived microRNAs in KSHV-associated malignancies. *PLoS Pathog.* **2013**, *9*, No. e1003484.
(13) McNamara, R. P.; Chugh, P. E.; Bailey, A.; Costantini, L. M.; Ma, Z.; Bigi, R.; Cheves, A.; Eason, A. B.; Landis, J. T.; Host, K. M.; Xiong, J.; Griffith, J. D.; Damania, B.; Dittmer, D. P. Extracellular vesicles from Kaposi Sarcoma-associated herpesvirus lymphoma induce long-term endothelial cell reprogramming. *PLoS Pathog.* **2019**, *15*, No. e1007536.
(14) Bogerd, H. P.; Whisnant, A. W.; Kennedy, E. M.; Flores, O.; Cullen, B. R. Derivation and characterization of Dicer- and microRNA-deficient human cells. *RNA* **2014**, *20*, 923−937.
(15) McNamara, R. P.; Caro-Vegas, C. P.; Costantini, L. M.; Landis, J. T.; Griffith, J. D.; Damania, B. A.; Dittmer, D. P. Large-scale, cross-flow based isolation of highly pure and endocytosis-competent extracellular vesicles. *J. Extracell. Vesicles* **2018**, *7*, 1541396.
(16) Shah, S.; Chandra, A.; Kaur, A.; Sabnis, N.; Lacko, A.; Gryczynski, Z.; Fudala, R.; Gryczynski, I. Fluorescence properties of doxorubicin in PBS buffer and PVA films. *J. Photochem. Photobiol., B* **2017**, *170*, 65−69.
(17) Meckes, D. G., Jr.; Raab-Traub, N. Microvesicles and viral infection. *J. Virol.* **2011**, *85*, 12844−12854.
(18) Verweij, F. J.; Revenu, C.; Arras, G.; Dingli, F.; Loew, D.; Pegtel, D. M.; Follain, G.; Allio, G.; Goetz, J. G.; Zimmermann, P.; Herbomel, P.; Del Bene, F.; Raposo, G.; van Niel, G. Live Tracking of Inter-organ Communication by Endogenous Exosomes In Vivo. *Dev. Cell* **2019**, *48*, 573−589.
(19) Théry, C.; Witwer, K. W.; Aikawa, E.; Alcaraz, M. J.; Anderson, J. D.; Andriantsitohaina, R.; Antoniou, A.; Arab, T.; Archer, F.; Atkin-Smith, G. K.; Ayre, D. C.; Bach, J. M.; Bachurski, D.; Baharvand, H.; Balaj, L.; Baldacchino, S.; Bauer, N. N.; Baxter, A. A.; Bebawy, M.; Beckham, C.; Bedina Zavec, A.; Benmoussa, A.; Berardi, A. C.; Bergese, P.; Bielska, E.; Blenkiron, C.; Bobis-Wozowicz, S.; Boilard, E.; Boireau, W.; Bongiovanni, A.; Borràs, F. E.; Bosch, S.; Boulanger, C. M.; Breakefield, X.; Breglio, A. M.; Brennan, M.; Brigstock, D. R.; Brisson, A.; Broekman, M. L.; Bromberg, J. F.; Bryl-Górecka, P.; Buch, S.; Buck, A. H.; Burger, D.; Busatto, S.; Buschmann, D.; Bussolati, B.; Buzás, E. I.; Byrd, J. B.; Camussi, G.; Carter, D. R.; Caruso, S.; Chamley, L. W.; Chang, Y. T.; Chen, C.; Chen, S.; Cheng, L.; Chin, A. R.; Clayton, A.; Clerici, S. P.; Cocks, A.; Cocucci, E.; Coffey, R. J.; Cordeiro-da-Silva, A.; Couch, Y.; Coumans, F. A.; Coyle, B.; Crescitelli, R.; Criado, M. F.; D'Souza-Schorey, C.; Das, S.; Datta Chaudhuri, A.; de Candia, P.; De Santana, E. F.; De Wever, O.; Del Portillo, H. A.; Demaret, T.; Deville, S.; Devitt, A.; Dhondt, B.; Di Vizio, D.; Dieterich, L. C.; Dolo, V.; Dominguez Rubio, A. P.; Dominici, M.; Dourado, M. R.; Driedonks, T. A.; Duarte, F. V.; Duncan, H. M.; Eichenberger, R. M.; Ekström, K.; El Andaloussi, S.; Elie-Caille, C.; Erdbrügger, U.; Falcón-Pérez, J. M.; Fatima, F.; Fish, J. E.; Flores-Bellver, M.; Försönits, A.; Frelet-Barrand, A.; Fricke, F.; Fuhrmann, G.; Gabrielsson, S.; Gámez-Valero, A.; Gardiner, C.; Gärtner, K.; Gaudin, R.; Gho, Y. S.; Giebel, B.; Gilbert, C.; Gimona, M.; Giusti, I.; Goberdhan, D. C.; Görgens, A.; Gorski, S. M.; Greening, D. W.; Gross, J. C.; Gualerzi, A.; Gupta, G. N.; Gustafson, D.; Handberg, A.; Haraszti, R. A.; Harrison, P.; Hegyesi, H.; Hendrix, A.; Hill, A. F.; Hochberg, F. H.; Hoffmann, K. F.; Holder, B.; Holthofer, H.; Hosseinkhani, B.; Hu, G.; Huang, Y.; Huber, V.; Hunt, S.; Ibrahim, A. G.; Ikezu, T.; Inal, J. M.; Isin, M.; Ivanova, A.; Jackson, H. K.; Jacobsen, S.; Jay, S. M.; Jayachandran, M.; Jenster, G.; Jiang, L.; Johnson, S. M.; Jones, J. C.; Jong, A.; Jovanovic-Talisman, T.; Jung, S.; Kalluri, R.; Kano, S. I.; Kaur, S.; Kawamura, Y.; Keller, E. T.; Khamari, D.; Khomyakova, E.; Khvorova, A.; Kierulf, P.; Kim, K. P.; Kislinger, T.; Klingeborn, M.; Klinke, D. J.; Kornek, M.; Kosanović, M. M.; Kovács, A.; Krämer-Albers, E. M.; Krasemann, S.; Krause, M.; Kurochkin, I. V.; Kusuma, G. D.; Kuypers, S.; Laitinen, S.; Langevin, S. M.; Languino, L. R.; Lannigan, J.; Lässer, C.; Laurent, L. C.; Lavieu, G.; Lázaro-Ibáñez, E.; Le Lay, S.; Lee, M. S.; Lee, Y. X. F.; Lemos, D. S.; Lenassi, M.; Leszczynska, A.; Li, I. T.; Liao, K.; Libregts, S. F.; Ligeti, E.; Lim, R.; Lim, S. K.; Linē, A.; Linnemannstöns, K.; Llorente, A.; Lombard, C. A.; Lorenowicz, M. J.; Lörincz, Á.; Lötvall, J.; Lovett, J.; Lowry, M. C.; Loyer, X.; Lu, Q.; Lukomska, B.; Lunavat, T. R.; Maas, S. L.; Malhi, H.;

https://doi.org/10.1021/acsbiomedchemau.1c00030
ACS Bio Med Chem Au 2022, 2, 140−149

Marcilla, A.; Mariani, J.; Mariscal, J.; Martens-Uzunova, E. S.; Martin-Jaular, L.; Martinez, M. C.; Martins, V. R.; Mathieu, M.; Mathivanan, S.; Maugeri, M.; McGinnis, L. K.; McVey, M. J.; Meckes, D. G.; Meehan, K. L.; Mertens, I.; Minciacchi, V. R.; Möller, A.; Møller Jørgensen, M.; Morales-Kastresana, A.; Morhayim, J.; Mullier, F.; Muraca, M.; Musante, L.; Mussack, V.; Muth, D. C.; Myburgh, K. H.; Najrana, T.; Nawaz, M.; Nazarenko, I.; Nejsum, P.; Neri, C.; Neri, T.; Nieuwland, R.; Nimrichter, L.; Nolan, J. P.; Nolte-'t Hoen, E. N.; Noren Hooten, N.; O'Driscoll, L.; O'Grady, T.; O'Loghlen, A.; Ochiya, T.; Olivier, M.; Ortiz, A.; Ortiz, L. A.; Osteikoetxea, X.; Østergaard, O.; Ostrowski, M.; Park, J.; Pegtel, D. M.; Peinado, H.; Perut, F.; Pfaffl, M. W.; Phinney, D. G.; Pieters, B. C.; Pink, R. C.; Pisetsky, D. S.; Pogge von Strandmann, E.; Polakovicova, I.; Poon, I. K.; Powell, B. H.; Prada, I.; Pulliam, L.; Quesenberry, P.; Radeghieri, A.; Raffai, R. L.; Raimondo, S.; Rak, J.; Ramirez, M. I.; Raposo, G.; Rayyan, M. S.; Regev-Rudzki, N.; Ricklefs, F. L.; Robbins, P. D.; Roberts, D. D.; Rodrigues, S. C.; Rohde, E.; Rome, S.; Rouschop, K. M.; Rughetti, A.; Russell, A. E.; Saá, P.; Sahoo, S.; Salas-Huenuleo, E.; Sánchez, C.; Saugstad, J. A.; Saul, M. J.; Schiffelers, R. M.; Schneider, R.; Schøyen, T. H.; Scott, A.; Shahaj, E.; Sharma, S.; Shatnyeva, O.; Shekari, F.; Shelke, G. V.; Shetty, A. K.; Shiba, K.; Siljander, P. R.; Silva, A. M.; Skowronek, A.; Snyder, O. L.; Soares, R. P.; Sódar, B. W.; Soekmadji, C.; Sotillo, J.; Stahl, P. D.; Stoorvogel, W.; Stott, S. L.; Strasser, E. F.; Swift, S.; Tahara, H.; Tewari, M.; Timms, K.; Tiwari, S.; Tixeira, R.; Tkach, M.; Toh, W. S.; Tomasini, R.; Torrecilhas, A. C.; Tosar, J. P.; Toxavidis, V.; Urbanelli, L.; Vader, P.; van Balkom, B. W.; van der Grein, S. G.; Van Deun, J.; van Herwijnen, M. J.; Van Keuren-Jensen, K.; van Niel, G.; van Royen, M. E.; van Wijnen, A. J.; Vasconcelos, M. H.; Vechetti, I. J.; Veit, T. D.; Vella, L. J.; Velot, É.; Verweij, F. J.; Vestad, B.; Viñas, J. L.; Visnovitz, T.; Vukman, K. V.; Wahlgren, J.; Watson, D. C.; Wauben, M. H.; Weaver, A.; Webber, J. P.; Weber, V.; Wehman, A. M.; Weiss, D. J.; Welsh, J. A.; Wendt, S.; Wheelock, A. M.; Wiener, Z.; Witte, L.; Wolfram, J.; Xagorari, A.; Xander, P.; Xu, J.; Yan, X.; Yáñez-Mó, M.; Yin, H.; Yuana, Y.; Zappulli, V.; Zarubova, J.; Žėkas, V.; Zhang, J. Y.; Zhao, Z.; Zheng, L.; Zheutlin, A. R.; Zickler, A. M.; Zimmermann, P.; Zivkovic, A. M.; Zocco, D.; Zuba-Surma, E. K. Minimal information for studies of extracellular vesicles 2018 (MISEV2018): a position statement of the International Society for Extracellular Vesicles and update of the MISEV2014 guidelines. *J. Extracell. Vesicles* **2018**, *7*, 1535750.

(20) Chen, X.; Wang, X.; Wang, Y.; Yang, L.; Hu, J.; Xiao, W.; Fu, A.; Cai, L.; Li, X.; Ye, X.; Liu, Y.; Wu, W.; Shao, X.; Mao, Y.; Wei, Y.; Chen, L. Improved tumor-targeting drug delivery and therapeutic efficacy by cationic liposome modified with truncated bFGF peptide. *J. Controlled Release* **2010**, *145*, 17−25.

(21) Kim, M. S.; Haney, M. J.; Zhao, Y.; Mahajan, V.; Deygen, I.; Klyachko, N. L.; Inskoe, E.; Piroyan, A.; Sokolsky, M.; Okolie, O.; Hingtgen, S. D.; Kabanov, A. V.; Batrakova, E. V. Development of exosome-encapsulated paclitaxel to overcome MDR in cancer cells. *Nanomedicine* **2016**, *12*, 655−664.

(22) Cavallin, L. E.; Ma, Q.; Naipauer, J.; Gupta, S.; Kurian, M.; Locatelli, P.; Romanelli, P.; Nadji, M.; Goldschmidt-Clermont, P. J.; Mesri, E. A. KSHV-induced ligand mediated activation of PDGF receptor-alpha drives Kaposi's sarcomagenesis. *PLoS Pathog.* **2018**, *14*, No. e1007175.

(23) Baker, G. E.; Reeset, B. E. Chapter 12 Using Confocal Laser Scanning Microscopy to Investigate the Organization and Development of Neuronal Projections Labeled with DiI. *Methods Cell Biol.* **1993**, *38*, 325−344.

(24) McNamara, R. P.; Costantini, L. M.; Myers, T. A.; Schouest, B.; Maness, N. J.; Griffith, J. D.; Damania, B. A.; MacLean, A. G.; Dittmer, D. P. Nef Secretion into Extracellular Vesicles or Exosomes Is Conserved across Human and Simian Immunodeficiency Viruses. *mBio* **2018**, *9*, No. e02344.

(25) Stearns, V.; Mori, T.; Jacobs, L. K.; Khouri, N. F.; Gabrielson, E.; Yoshida, T.; Kominsky, S. L.; Huso, D. L.; Jeter, S.; Powers, P.; Tarpinian, K.; Brown, R. J.; Lange, J. R.; Rudek, M. A.; Zhang, Z.; Tsangaris, T. N.; Sukumar, S. Preclinical and clinical evaluation of intraductally administered agents in early breast cancer. *Sci. Transl. Med.* **2011**, *3* (106), 106ra108.

(26) Folkman, J. Tumor angiogenesis: therapeutic implications. *N. Engl. J. Med.* **1971**, *285*, 1182−1186.

(27) Northfelt, D. W.; Dezube, B. J.; Thommes, J. A.; Miller, B. J.; Fischl, M. A.; Friedman-Kien, A.; Kaplan, L. D.; Du Mond, C.; Mamelok, R. D.; Henry, D. H. Pegylated-liposomal doxorubicin versus doxorubicin, bleomycin, and vincristine in the treatment of AIDS-related Kaposi's sarcoma: Results of a randomized phase III clinical trial. *J. Clin. Oncol.* **1998**, *16*, 2445−2451.

(28) Udhrain, A.; Skubitz, K. M.; Northfelt, D. W. Pegylated liposomal doxorubicin in the treatment of AIDS-related Kaposi's sarcoma. *Int. J. Nanomed.* **2007**, *2*, 345−352.

(29) Zhang, C. G.; Zhu, W. J.; Liu, Y.; Yuan, Z. Q.; Yang, S. D.; Chen, W. L.; Li, J. Z.; Zhou, X. F.; Liu, C.; Zhang, X. N. Novel polymer micelle mediated co-delivery of doxorubicin and P-glycoprotein siRNA for reversal of multidrug resistance and synergistic tumor therapy. *Sci. Rep.* **2016**, *6*, 23859.

(30) Gradishar, W. J.; Tjulandin, S.; Davidson, N.; Shaw, H.; Desai, N.; Bhar, P.; Hawkins, M.; O'Shaughnessy, J. Phase III trial of nanoparticle albumin-bound paclitaxel compared with polyethylated castor oil-based paclitaxel in women with breast cancer. *J. Clin. Oncol.* **2005**, *23*, 7794−7803.

(31) Sancho-Albero, M.; Navascués, N.; Mendoza, G.; Sebastián, V.; Arruebo, M.; Martín-Duque, P.; Santamaría, J. Exosome origin determines cell targeting and the transfer of therapeutic nanoparticles towards target cells. *J. Nanobiotechnol.* **2019**, *17*, 16.

(32) Rivera-Serrano, E. E.; González-López, O.; Das, A.; Lemon, S. M., Cellular entry and uncoating of naked and quasi-enveloped human hepatoviruses. *Elife* **2019**, *8*. DOI: 10.7554/eLife.43983

(33) Choi, H.; Choi, Y.; Yim, H. Y.; Mirzaaghasi, A.; Yoo, J.-K.; Choi, C. Biodistribution of Exosomes and Engineering Strategies for Targeted Delivery of Therapeutic Exosomes. *Tissue Eng. Regener. Med.* **2021**, *18*, 499−511.

(34) Rivera-Serrano, E. E.; Gonzalez-Lopez, O.; Das, A.; Lemon, S. M. Cellular entry and uncoating of naked and quasi-enveloped human hepatoviruses. *Elife* **2019**, *8*, No. e43983.

(35) Das, A.; Barrientos, R.; Shiota, T.; Madigan, V.; Misumi, I.; McKnight, K. L.; Sun, L.; Li, Z.; Meganck, R. M.; Li, Y.; Kaluzna, E.; Asokan, A.; Whitmire, J. K.; Kapustina, M.; Zhang, Q.; Lemon, S. M. Gangliosides are essential endosomal receptors for quasi-enveloped and naked hepatitis A virus. *Nat. Microbiol.* **2020**, *5*, 1069−1078.

(36) Caby, M.-P.; Lankar, D.; Vincendeau-Scherrer, C.; Raposo, G.; Bonnerot, C. Exosomal-like vesicles are present in human blood plasma. *Int. Immunol.* **2005**, *17*, 879−887.

(37) Mohamed, M.; Abu Lila, A. S.; Shimizu, T.; Alaaeldin, E.; Hussein, A.; Sarhan, H. A.; Szebeni, J.; Ishida, T. PEGylated liposomes: immunological responses. *Sci. Technol. Adv. Mater.* **2019**, *20*, 710−724.

https://doi.org/10.1021/acsbiomedchemau.1c00030
ACS Bio Med Chem Au 2022, 2, 140−149